Analysis and Modeling of wireless battery charger using PCB coreless transformer and Class E inverter

Ihsen Jabri
Université de Tunis El Manar, ENIT-L.S.E, BP 37-1002, Tunis le Belvédère,

Adel Bouallegue
Université de Sousse, ENISO-SAGE, Sousse, Tunisie

Fethi Ghodbane
Université de Tunis El Manar, ENIT-L.S.E, BP 37-1002, Tunis le Belvédère

Abstract— This paper focuses on the application of a wireless power transfer technology in an electric vehicle battery charger. The appropriate application is based on the using of a coreless transformer that is composed of two separated core. A primary circuit integrated in the parking platform and a secondary circuit implemented in the vehicle. The modeling methodology needs to provide guidelines in the selection of system performance values and design parameters. A sensitivity analysis for several blocks of the wireless charger system including fundamental concept of coreless PCB transformer, Class-E inverter, resonant converter, electric motor and battery are performed. Simulations results are reported to conclude about the choice of the required design. The issues of coil misalignment, highlighted in wireless charging, can degrade efficiency, reduce power transfer and extend charging time. Control system is investigated to detect and adjust car position.

***Index Terms*— Wireless, Coreless transformer, Electric Vehicle, Methodology**

1. INTRODUCTION

Recently, Wireless power transmission WPT using magnetic fields has reaped considerable attention due to their promises of offering interest economic, environmental sustainability protection, safety and flexibility for several applications. Resonant inductive coupling power transfer is an emerging technique, which enables power transfer to loads through air. The concept of this technique is based on the use of a coreless transformer in addition to capacitors in series or in parallel in the magnetic circuits to compensate losses. The fact that the primary and secondary coils are granted at the same frequency generates a resonance phenomenon. Regarding the several advantages associated with the WPT, the use of this technology in the electric vehicle battery's charging application is considered [1-2]. A lot of interesting researches were accomplished in this wireless charging mode with various innovative techniques as illustrate in TABLE I [3-4-5-6].

Coreless transformer offers various advantages such as low costs, very high power density, no magnetic loss and ease of manufacture. PCBs with coreless transformers are particularly suited for use in applications where strict height requirements must be met. In the modeling of PCB coreless transformer various parameters affects on their optimization characteristic where the modeling becomes not a trivial task. The influence of each parameter is analyzed to deduce the tendencies and then make a choice. This paper is intended to study the effect of different geometric and electric parameters in order to model the proposed wireless battery charger system for electric vehicle application. Several analyses are carried out as well as simulations results are reported to conclude about the choice of the desired design. A control system based on the use of microcontroller is developed for proximity sensing and automating to tackle the impact of misalignment between transmitter and receiver coil.

TABLE I. The most interesting researchers accomplished in wireless power transfer applicable in EV

Researchers & developers	Air gap [cm]	Power [kw]	[%]
Partners for Advance Transit and Highways (PATH)	7.6	60	60
Auckland University	20	5	90
Kaist,1G OLEV	1	3	80
Kaist 2G OLE	17	6	72
Kaist 3G OLEV ; Bus	17	60	71
Kaist 3G OLEV;Suvs	17	20	83
Waseda advanced Electric Bus	10	30	92
WiTricity with MIT	18	3.3	90
Univ of Michigan, Dearborn	20	8	95.7
Laboratory (ORNL) ,US	7.5	7	90
PLUGLESS™ , Evatran Group	10	3.3	88.8

2. ANALYSIS OF PCB CORELESS TRANSFORMER

A. Mathematical modeling of PCB parameter

According to the literature, there are several geometries circular, rectangular, hexagonal, and octagonal. In this study, a planar coil with a rectangular geometry is considered because it offers better tolerance to misalignment between the primary and secondary windings of the coreless transformer [7].

This section provides some analytical solutions used in the calculation of inductance, capacitors and resistors of coreless PCB transformer. This method of calculation is more efficient and easiest than finite element analysis (FEA) method. In case of rectangular spiral inductor, Mohan et al consider «Greenhouse formula » equation to estimate the value of inductance L presented as follow [8].

$$L = \frac{1.27\mu_0 N^2(do-di)}{2}\left(\ln\left(\frac{2.07}{\frac{do-di}{do+di}}\right) + 0.18\left(\frac{do-di}{do+di}\right) + 0.13\left(\frac{do-di}{do+di}\right)^2\right) \quad (1)$$

Were N is the number of turns, do is the outer diameter, di is the inner diameter of the coil.

The winding resistance, R_s increases with the operating frequency due to skin effect δ which is given as following expression

$$\delta = \sqrt{\frac{\rho_c}{\pi f \mu_0}} \quad (2)$$

In addition, the resistance Rs is expressed as

$$Rs = \rho_c \frac{l_c}{wt_c} * \frac{t_c}{\delta\left(1 - e^{\frac{-t_c}{\delta}}\right)} \quad (3)$$

The coreless PCB transformers capacities are calculated assuming that the two conductive coils are planar and parallel. Parallel total capacity, Cp is given as

$$C_p = C_{pc} + C_{ps} = (\alpha\, \varepsilon_{rc} + \beta\, \varepsilon_{rs}) \frac{\varepsilon_0 t_c}{s} l_g \quad (4)$$

The width of the coil is also important in determining the inductance. Thus, if the width is small, the resistance is important thereby reducing the quality factor of the coil and then inductance. TABLE II groups all parameters used in calculation of winding resistance and capacitors.

TABLE II. MATHEMATICALLY PARAMETERS USED IN WINDING RESISTANCE AND CAPACITOR EQUATION

ρc	Conductivity = 17,24.10^-9	ε_0	permittivity =8.854e^{-12}
lc	Length of the conductive path lc =4*N*(do-w)-(s+w)*(2N+1)^2	lg	length of the air gap lg = 4*(do-N*w)*(N-1)-4*s*N*(N+1)
ε_{rs}	dielectric constant of FR4 material=4.4	ε_{rc}	dielectric constant of the layer
tc	Thickness	w	Width of the conductor
μ_0	Permeability=4π10^-7	β	0,1
f	Frequency	α	0,9

B. Effect of Geometric parameter

The inductor parameters can be classified into two groups: Technology and layout parameters. Technological parameters such as substrate thickness, silicon dioxide and layer thickness depend on the manufacturing process. The available optimization parameters are the number of turns N, the width of the conductor ω, the spacing between adjacent conductors, s, and the outer diameter, do. A sufficiently large number of turns ensure to have a good efficiency and an important quality factor. Since the resistivity of metal is fixed by the technology and the width and length are set to obtain the desired inductance, the only way to reduce the direct current resistance is by changing the thickness of the metal. A higher thickness trace implies a lower resistance, which increases the quality factor. The magnetizing inductance and the leakage inductances of PCB coreless transformer depend on the dimensions of the primary and secondary system and the air gap length. For the given power transfer application, the coupling coefficient can be improved by increasing the area of the transformer. However, if the area of the transformer is increased by increasing the number of turns, the rate of increase of the transformers self inductance is higher in comparison to its leakage inductance which leads to high coupling coefficient.

3. ANALYSES OF CLASS-E INVERTER

The bloc diagram of the proposed wireless charger system for electric vehicle is illustrated in Fig.1

The duty cycle D is given by

$$D = 1 - \frac{V_{in}(1+n)}{v_{out}} \quad (5)$$

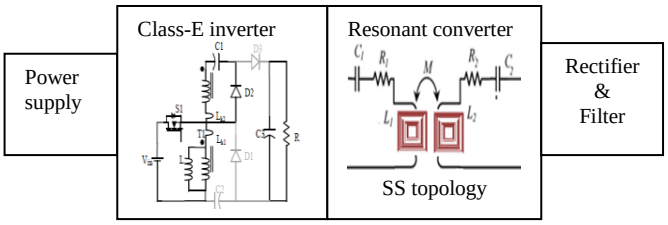

Fig.1 Bloc diagram of the proposed wireless charger battery system

Where V_{in} is the input Voltage, V_{out} is the Output Voltage and n is the transformer turns ratio.

The magnetizing inductance L_m has to be greater than the boundary magnetizing inductance introduced as

$$L_m > \frac{D}{2}\left(\frac{1-D}{1+n}\right)^2 \frac{R}{f} \quad (6)$$

The breakdown voltage B_v of the MOSFET is presented as

$$B_v = \frac{V_{cc}}{s_F}\left(\frac{\pi^2}{4} + 1\right) \quad (7)$$

Where S_F is the safety factor whose value is chosen to be equal to 0.8 (less than 1) and V_{cc} is the supply voltage of the class E power amplifier.

The full load resistance is equal to

$$R_L = \frac{8{V_{cc}}^2}{(\pi^2+4)P} \quad (8)$$

Where P is the output power of the amplifier and is fixed by the designer.

The current drawn from the DC power supply is

$$I_0 = \frac{P}{V_{cc}} \quad (9)$$

The value of the shunt capacitance C_1 is presented as

$$C_1 = \frac{1}{\omega R_L\left(\frac{\pi^2}{4}+1\right)\frac{\pi}{2}} \quad (10)$$

The value of C_2 is calculated by using the equation below

$$C_2 = \frac{1}{\omega R_L\left(Q-(\pi^2-4)\frac{\pi}{16}\right)} \quad (11)$$

Where Q presents the quality factor.

Usually the value of ωL_1 is chosen to be 30 or more than times the unadjusted value of ωC_1. Thus

$$L_1 > \frac{30}{\omega^2 C_1} \quad (12)$$

The value of L_2 is found from the equation below

$$L_2 = Q\frac{R_L}{\omega} \quad (13)$$

4. ANALYSIS OF RESONANT CONVERTER

The secondary current $i_2(t)$ is sinusoidal with peak amplitude and phase shift φ, and is can be introduced as

$$i_2(t) = I_2 \sin(\omega_s t - \varphi) \quad (14)$$

The secondary voltage $u_2(t)$ is expressed as

$$u_2(t) = \frac{4U_L}{\pi} \sin(\omega_s t - \varphi) \quad (15)$$

The sinusoidal output current $i_2(t)$ is rectified by a diode bridge rectifier, and next is filtered by a capacitor C_F. Thus, the dc component of $|i_2(t)|$ is equal to load current I_L.

$$I_L = \frac{2}{\pi} I_2 \quad (16)$$

Consequently, the effective load resistance is written as

$$R_{eff} = \frac{8U_L}{\pi^2 I_L} = \frac{8}{\pi^2} R_L \quad (17)$$

The reflected secondary side impedance for SS compensation expressed as:

$$Z_{ref} = \frac{\omega^2 M^2}{R_{es} + j\omega L_2 + \frac{1}{j\omega C_2}} \quad (18)$$

The values of reflected impedances are strongly depended on coupling coefficient and decreasing when the coupling coefficient is lower smaller.

The desired resonant capacitor is given by

$$C_1 = \frac{L_2}{L_1} C_2 \quad (19)$$

Therefore, the equivalent impedance seen by the power supply for a SS topology is given by

$$Z_{eq} = R_1 + j\omega L_1 + \frac{1}{j\omega C_1} + \frac{\omega^2 M^2}{R_{eff} + j\omega L_2 + \frac{1}{j\omega C_2}} \quad (20)$$

The power transfer efficiency without compensation is written as

$$\eta = \frac{R_L}{R_{eff} + R_1\left(\frac{R_{eff} + j\omega(L_2 + M)}{j\omega M}\right)} \quad (21)$$

The power transfer efficiency with SS compensation is calculated as

$$\eta_C = \frac{R_L}{R_{eff} + R_1\left(\frac{R_{eff}}{j\omega M}\right)} \quad (22)$$

Fig.2 illustrated the coreless transformer power transfer efficiency with and without SS capacitive compensation. Without compensation, the maximum power transfer efficiency is 78.14% while with capacitive compensation is equal to 93.18%. Simulation results proved that, with SS capacitive compensation the power transfer efficiency is enhanced with a rate of 15.04%.

The high secondary leakage inductance, which causes a voltage drop and limitation of the transfer power range, presents an important issue in the WPT system. Consequently, primary winding compensation is needed to minimize the VA rating of the supply and secondary winding compensation is required to enhance the power transfer efficiency. The maximum efficiency depends on the coupling coefficient between resonators. In order to achieve acceptable efficiency in relative distance of lager, it is necessary to have resonator coils with high coupling coefficient.

The power transfer from primary side trough the air gap to secondary side can be expressed as a function of reflected resistance multiplied by the square of primary current

$$P = REL(Z_{ref}) I_1^2 \quad (23)$$

The transferred power for the SS compensation topology versus normalized frequency fs/fo, and for different values of load resistance RL are depicted in Fig. 3.

It is lucid that the transferred power are strongly depended on coupling coefficient and very sensitive to the increasing of load resistance.

The quality factor Q presents also important parameters that affect on the modeling of the WPT system. The primary quality factor depends on the geometry of the primary winding transformer and the required primary current and the secondary quality factor affect on the power transfer efficiency.

The coreless transformer operates under lower and variable magnetic coupling factor *k*. In addition, the voltage gain G_V defined as a function of *k*, Q and operating frequency can be rewritten as follows:

$$G_V = \frac{K\omega^2}{Q}^{0.5} \sqrt{\left(\frac{\omega^2 + K - 1}{Q}\right)^2 + \left(\frac{K\omega^4 + \omega^4 - \omega^2 - K}{2\omega}\right)^2} \quad (24)$$

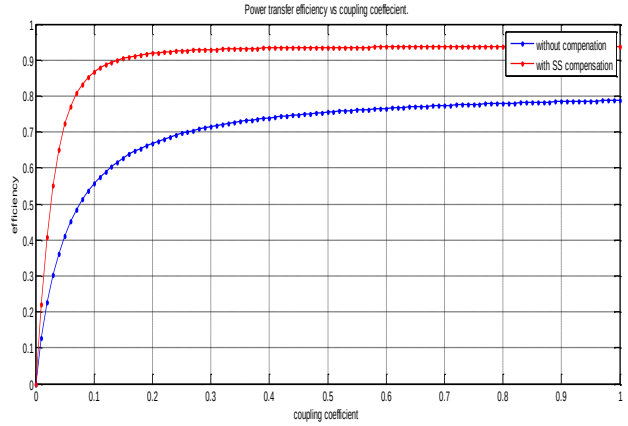

Fig. 2. Transfer power efficiency as a function of coupling coefficient with and without SS compensation

a)

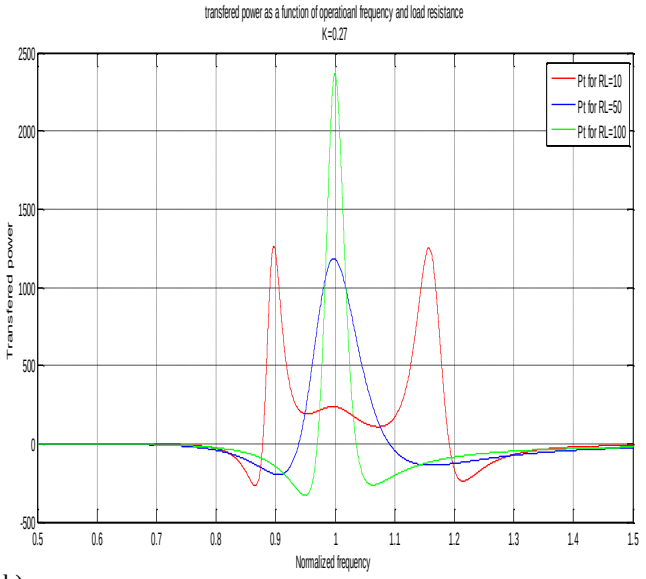

b)

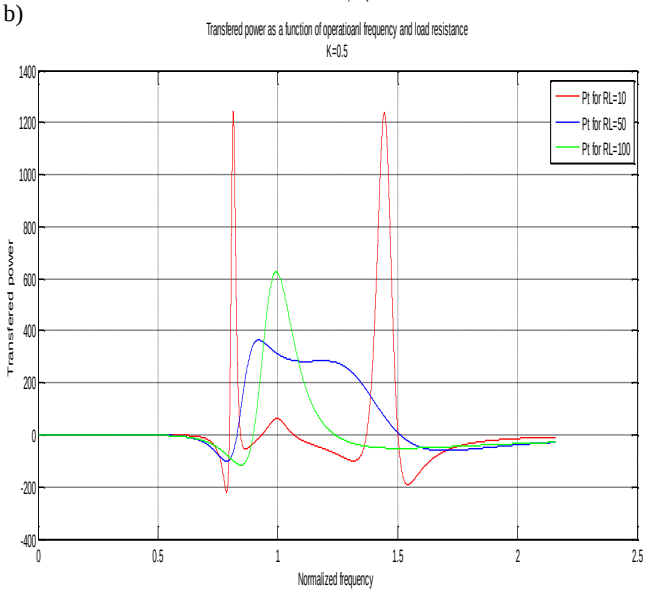

Fig. 3. Transferred power as a function of normalized frequency and load resistance R_L, for a) K=0.27 .b) K=0.5

Fig.4 illustrates the variation of voltage gain as function of frequency and quality factor for two various value of coupling coefficient K= 0.2 and K=0.7 .
Simulation results demonstrate that both figures have the same behavior save that for a low deviation in low *Q*.
At the resonance frequency $\omega=\omega 0$, the voltage gain Gv is equal to a unity and the current and the voltage of the resonant converter are in phase reducing thus reactive power. As the converter is functioning at this frequency, the current flowing through the magnetizing inductance is cancelled independently on coupling coefficient and load.
As shown in Fig.4, three important frequency regions can appear. A feedback regulator may be used to control the output voltage by choosing the corresponding range from these areas. Zone A is defined by small frequencies. The voltage gain G_V increases as the operational frequency increases. The unity gain frequency depends on coupling coefficient *k*. Zone B is the middle frequency region and is called the double-turned circuit. The gain largely depends on load variations and operational frequency. Zone C is defined by great frequencies. The voltage gain G_V decreases the operational frequency of the converter increases. Despite that the maximum voltage gain is obtained in the Range B, this region is very sensitive to load changes and coupling coefficient *k* and it has nonlinear characteristics versus operational frequency. In addition, it is complicated to control the output voltage. According to Range A and Range C the gain is a monotonic function of operational frequency so it is easy to control the output voltage. Range C is considered as the more advantageous region because the gain voltage for each load conditions is fewer responsive comparing to range A and fast changes in output voltage are noted when increasing frequency which is significant if danger state is detecting.

5. MODELING OF THE ELECTRIC CAR

The electric power (P_{ele}) required of the energy storage system is equal to the mechanical power (P_{mec}) plus the power consumed by the vehicle auxiliary systems (P_{aux}). Furthermore, the losses of the traction system through its total efficiency (ηt) must be considered. These losses depend on the direction of power.
The electric power is expressed as

$$P_{ele} = \frac{P_{mec}}{\eta_t} + P_{aux} \quad (25)$$

Where

$$P_{mec} = \frac{1}{2}\rho_{air}.A.C_{drag}.v^3.\text{sign}(v) + \mu_{rr}.m.g.v.\text{sign}(v) + K_{ri}m.a.v \quad (26)$$

Where v is the car speed
The constraint to dimension the electric motor is the accelerating from 0 to 45 km / h in 90 seconds for electric mode. Fig.6 shows that the power required to meet these constraints is about 1.4 kW. TABLE III groups all parameters used in calculation of electrical and mechanical power.

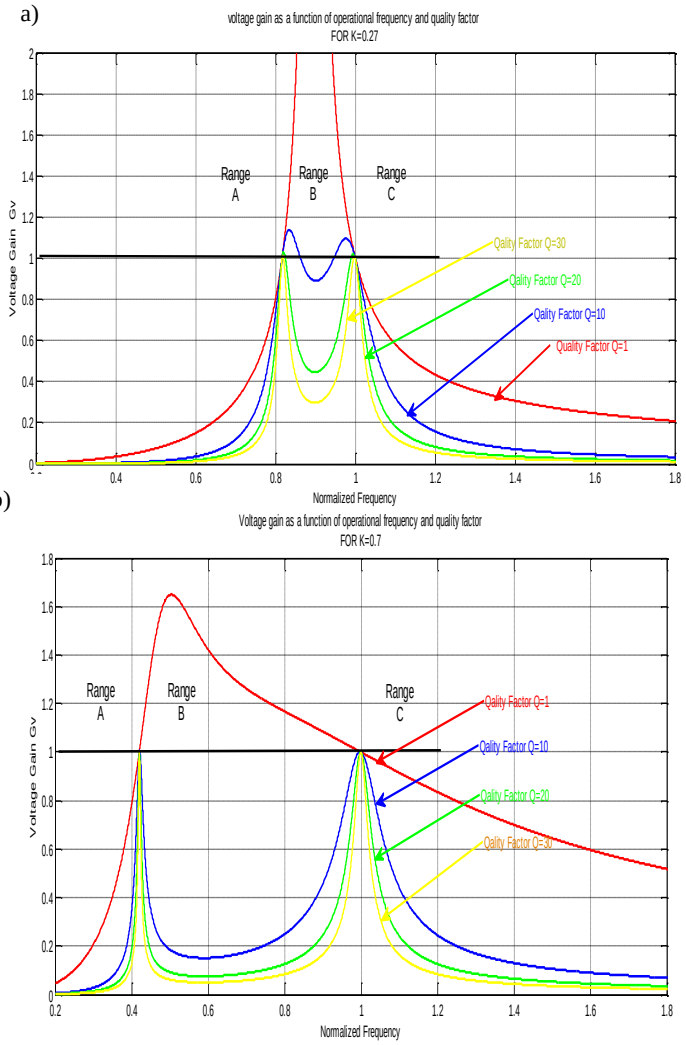

Fig. 4. Voltage gain as function of normalized frequency and quality factor for a) K= 0.2 .b) K=0.7

A. *Selection of the electric motor*

For this application a synchronous motor without brushes inductor with permanent magnets (PMSM) named JIANGSUWEHATSTONE CO., LTD is preferred. The proposed electric motor offers various advantages including performance as well as Light weight. This type of motor used in industrial equipment, power tools…, is powered by 48v battery, 1500w brushless DC motor.

TABLE III. PARAMETERS USED IN CALCULATION OF ELECTRICAL AND MECHANICAL POWER.

$\boldsymbol{\rho_{air}}$	Air density 1.25 kg/m3
$\boldsymbol{A}$	Frontal area for small car = $2m^2$
$\boldsymbol{C_{drag}}$	Drag coefficient for small car=0.3
$\boldsymbol{m}$	Mass =100kg
$\boldsymbol{g}$	Constant acceleration =9.80665 m/s2
$\boldsymbol{\mu_{rr}}$	Rolling resistance of the wheels =0.013
a	Acceleration of the vehicle.
$\boldsymbol{K_{ri}}$	Correction factor = 1.05
$\boldsymbol{P_{aux}}$	Auxiliary power 250W
$\boldsymbol{\eta_t}$	Efficiency =0.9

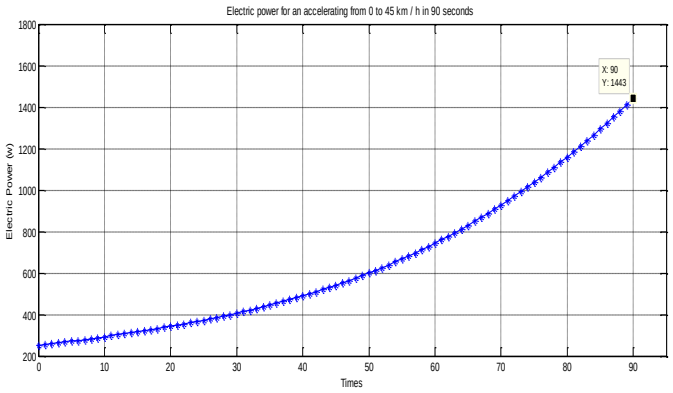

Fig. 6. Electric power required

B. Selection of the Battery

Many rechargeable batteries types differ from each other by several characteristics. At present, the majority of EVs are still equipped with Pb_acid battery, mainly for cost reasons. However, the Ni-MH batteries are becoming more common, especially in France where SAFT as one of the leading battery manufacturers, has carried out extensive research on these batteries specially adapted for EV. In addition for this application, a Ni-MH battery is used and their specifications are presented as following:

Rated voltage: 6 * 1.2V = 7.2V

Specific Energy: 50Wh / kg

Specific power: 1000w / kg

The target is to operate an electric motor for P_{abs} =1.5 kW, U=48V for time T=90s.

The current drawn by the motor is calculated as

$$I = \frac{P_{abs}}{U} = 1250\ A \quad (27)$$

The nominal capacity is expressed as

$$Q = I.T = 31.25\ \text{AH} \quad (28)$$

In addition, a 7.2V battery pack for nominal capacity 31.25 Ah is required.

6. MODELING OF PROPOSED WBC SYSTEM

Based on previous equations presented in the analyses of the wireless battery charger, it is easy to calculate all voltages, currents and electric component required to design the proposed system shown in Fig.7. Fig.9 models the iterative process applied in the designing of the appropriate system. If all conditions are reaches and all specifications are respected, the proposed model is willing to be defined In the first step, it is necessary to determine the geometric and electric parameters related to the coreless transformer: the dimension of the primary and secondary coils as well as the separation distance between them. Referring to analytic equations presented in the analyses of coreless transformer, it is easy to deduce provides inductors and electrical variables. According to the equations given in the analysis of the class-E inverter and SS resonant converter, the supply voltage, the resistance of the load R_L, the voltage necessary for the load and the transferred power can be determined and efficiency also can be calculated. At this point, a criterion of success is checked. The charging voltage should respect the specification given in the analyses of the EV battery. If the condition is unsatisfied, the designer ought to build a new geometry with a different set of parameters. If condition is satisfied, the desired design is achieved. The electrical parameters of the wireless battery charger are regrouped in Table IV.

7. CONTROL SYSTEM FOR MISALIGNMENT ISSUE

Fig.8 illustrates the control system simulated by ISIS Proteus software in order to detect and adjust the misalignment problem between transmitter and receiver coils. Detection is performed using linear Hall sensors mounted oppositely on the transmitter side, in order to sense the position of the receiver. Adjustment is recommended using visual notification about position of the electric car. A Hall sensor senses nearby magnetic field and generate a corresponding voltage which is interpreted by the micro-controller AT89C51 using ADC. In this simulation model, a voltage divider circuit acts as Hall sensor that produces a voltage. The microcontroller monitors the charging current level and causes automatic turning off wireless charging system whenever batter is fully charged and the charging current value decreases

8. CONCLUSION

In Wireless power transfer technology and precisely wireless charger battery (WBC) application, multi physics and highly variable parameters affect on the modeling of the appropriate system. A highly efficient wireless power transfer system is realized based on the using of Class-E inverter and a series series resonant converter. Analysis and modeling of the electric motor and NI-MH battery have been introduced. A control system performing the adjusting of car position in case of misalignment is also investigated.

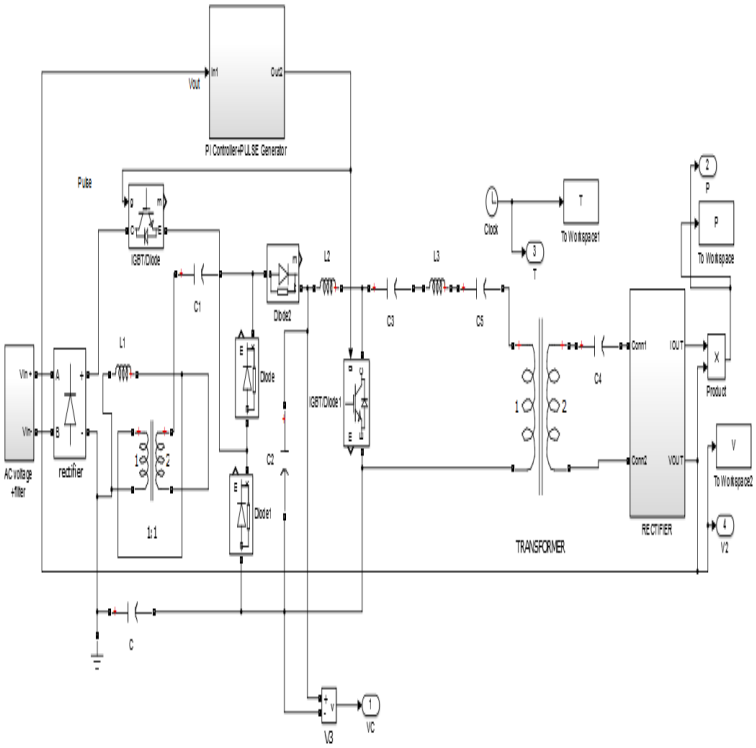

Fig.7 Matlab/simulink bloc diagram of the proposed WBC system

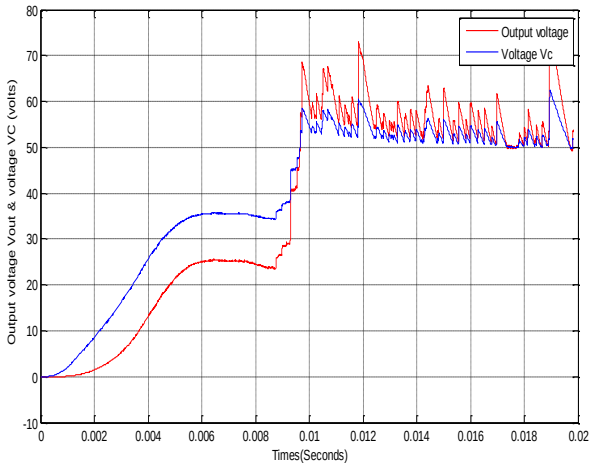

Fig.10 voltage across C3 capacitor and output voltage of the proposed WBC system

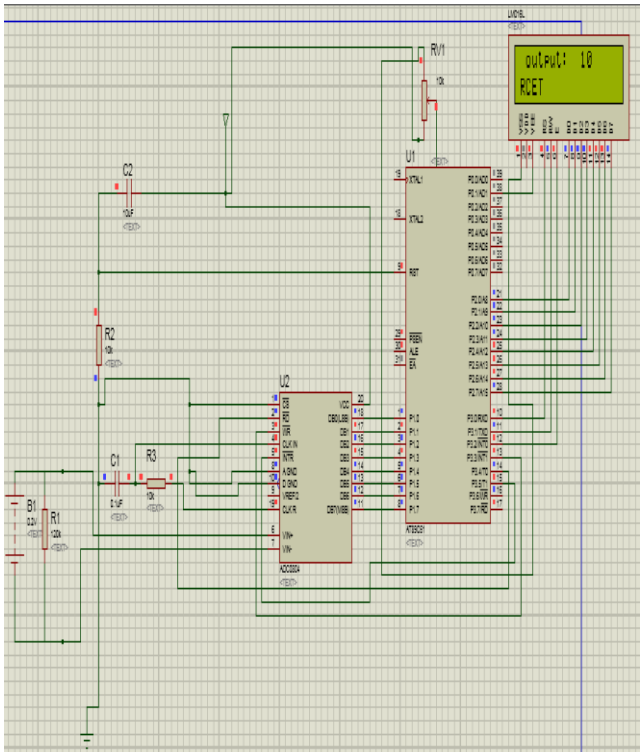

Fig.8 Control system for correction misalignment

TABLE IV. ELECTRIC PARAMETER OF THE PROPOSED WIRELESS BATTERY CHARGER SYSTEM FOR EV APPLICATION

Air gap	20mm
Dimension of primary coil	550mm X 550mm
Dimension of secondary coil	350mm X 350mm
Nb of turns	N1=30 N2=30
Frequency	50 kHz
Filter capacitor	Cf= 30µF
Primary and secondary resistance	R1=0.01Ω R2=0.01Ω
Primary and secondary capacitance	C1=23.6µF C2=23.6µF
Primary and secondary inductance	L1=38µH L2=38µH
Transferred power	1KW
Efficiency	0.91%
source voltage	100 V
Load resistance	RL=20Ω

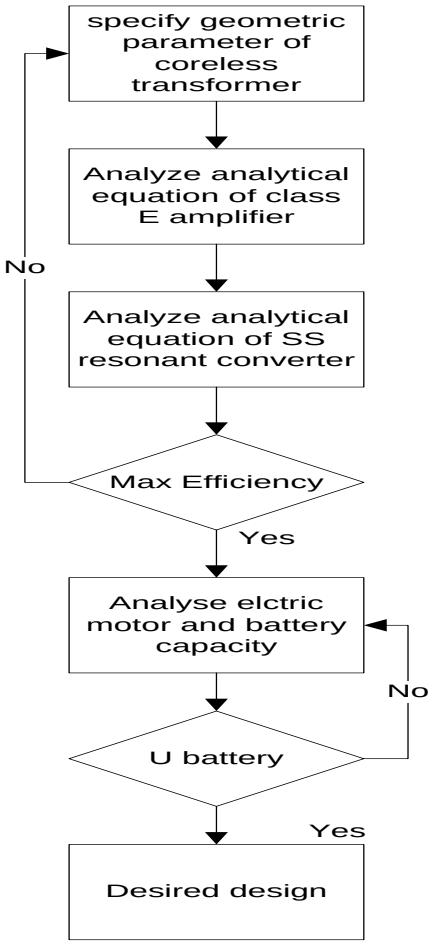

Fig.8 Iterative process applied to design proposed WBC system

9. REFERENCES

[1] Siqi Li, Chunting Chris Mi,"Wireless Power Transfer for Electric Vehicle Applications." IEEE Journal Of Emerging And Selected Topics In Power Electronics, Vol. 3, No. 1, March 2015.

[2] T.-D. Nguyen, S. Li, W. Li, and C. Mi, "Feasibility study on bipolar pads for efficient wireless power chargers," in Proc. APEC Expo., Fort Worth, TX, USA, 2014.

[3] N. Puqi, J. M. Miller, O. C. Onar, and C. P. White, "A compact wireless charging system development," in Proc. IEEE ECCE, Sep. 2013, pp. 3629–3634.

[4] Carlson, R. and Normann, B., "Test Results of the PLUGLESS™ Inductive Charging System from Evatran Group, Inc.," SAE Int. J. Alt. Power. / Volume 3, Issue 1 ,May 2014

[5] M. Budhia, J. T. Boys, G. A. Covic, and H. Chang-Yu, "Development of a single-sided flux magnetic coupler for electric vehicle IPT charging systems," IEEE Trans. Ind. Electron., vol. 60, no. 1, pp. 318–328, Jan. 2013.

[6] H. Jin, L. Wooyoung, C. Gyu-Hyeong, L. Byunghun, and R. Chun-Taek, "Characterization of novel inductive power transfer systems for on-line electric vehicles," in Proc. 26th Annu. IEEE APEC Expo, pp. 1975–1979, Mar. 2011

[7] N. Oodachi, K. Ogawa, H. Kudo, H. Shoki, S. Obayashi, T. Morooka, "Efficiency improvement of wireless power transfer via magnetic resonance using transmission coil array," IEEE International Symposium on Antennas and Propagation (APSURSI), 3-8 July 2011, pp. 1707-1710.

[8] B. Lenaerts, R. Puers, "Omnidirectional Inductive Powering for Biomedical Implants", Springer, 2009.